PCCP

Accepted Manuscript

ROYAL SOCIETY OF CHEMISTRY

www.rsc.org/pccp

Journal Name

ARTICLE

Branched isomeric 1,2,3-triazolium-based ionic liquids: New insight into structure-property relationships

Received 00th January 20xx,
Accepted 00th January 20xx

DOI: 10.1039/x0xx00000x

www.rsc.org/

M. Lartey,[a] J. Meyer-Ilse,[b] J. D. Watkins,[a] E. A. Roth,[a] S. Bowser,[c] V. A. Kusuma,[a] K. Damodaran,[c] X. Zhou,[a,d] M. Haranczyk,[e] E. Albenze,[a] D. R. Luebke,[a] D. Hopkinson,[a] J. B. Kortright,[b,*] H. B. Nulwala,[a,d, f*]

***E-mail**: J. B. Kortright (JBKortright@lbl.gov); H. B. Nulwala (hnulwala@andrew.cmu.edu)*

A series of four isomeric 1,2,3-triazolium-based ionic liquids (ILs) with varrying degree of branching were synthesized and characterized to investigate the effect of ion branching on thermal and physical properties of the resulting IL. It was found that increased branching led to a higher ionicity and higher viscosity. The thermal properties were also altered significantly and spectral changes in the near edge X-ray absorption fine structure (NEXAFS) spectra show that branching affects intermolecular interaction. While the ionicity and viscosity varying linearly with branching, the MDSC and NEXAFS measurements show that the cation shape has a stronger influence on the melting temperature and absorptive properties than the number of branched alkyl substituents.

Introduction

Room temperature ionic liquids (ILs) are organic salts which are liquids at room temperature. They are viewed as the solvents of the future due to their unique properties compared to traditional solvents, such as extreme low vapor pressure, non-flammability, high thermal stability and unique solvation potential.[1,2] Such attributes have already led to their use in a variety of industrial applications[3–5] such as solvents,[1,6,7] electrolytes,[8,9] and CO_2 capture.[6,10–12]

Ionic liquid properties are ultimately determined by a myriad of intra- and intermolecular interactions resulting from the tunable structural complexity of the molecular cations and anions. The choice of anion,[13] cation,[14] and the side groups[15,16] can alter the properties significantly through changing interactions. These interactions can include hydrogen bonding, Van der Waal's interactions, coulombic interactions, π-π interactions, and polarity.[17] The shape of the anion, cation, and their functional groups, and conformational differences in both the cation[18] and the anion[19–21] are also expected to affect the nature and magnitude of the interactions which can result in widely different physical and chemical properties.

Previously, we studied the effect of regioisomerism[22–25] and found that even subtle structural changes can have a dramatic effect on physical properties. For example, conformational flexibility[26] and hydrogen bonding[27,28] play an important role in thermal properties, while hydrogen bond-accepting and bond-donating ability can be used as a rough guide to elucidate interactions of the cation and anion.[29–31]

Our previous work, developing robust structure-property trends for ILs using a chemical informatics-based approach, revealed that short alkyl side chain branching tends to yield properties which were difficult to explain via simulations. This was mainly due to the increased viscosity and our inability to predict the densities correctly in a highly branched system.[23,24,32] To study the effect of branching and what influences the properties of these materials, we utilized Cu(I)-catalyzed click chemistry to synthesize 1,2,3-triazolium-based ILs. The click reaction products are regio-specific and provide excellent control over the chemistry. In addition, this chemistry tolerates the addition of a wide variety of functional groups.[33,34] The effects of various substitutions on the triazolium core on physical,[23] carbon capture,[24] and electrochemical[35] IL properties have been investigated.

In the present study, we utilize this chemistry to assemble isomeric cations to study how structure-property relationships evolve with

[a] *National Energy Technology Laboratory, P.O. Box 10940, Pittsburgh, PA, USA.*
[b] *Materials Science Division, Lawrence Berkeley National Laboratory, Berkeley, CA 94720, USA*
[c] *Department of Chemistry, University of Pittsburgh, Chevron Science Center, 219 Parkman Ave, Pittsburgh, PA 15260, USA*
[d] *Liquid Ion Solutions, LLC. 1817 Parkway View Drive, Pittsburgh, PA 15205, USA*
[e] *Computational Research Division, Lawrence Berkeley National Laboratory, Berkeley, CA 94720, USA*
[f] *Department of Chemistry, Carnegie Mellon University, 4400 Fifth Avenue, Pittsburgh, PA 15213, USA*
Electronic Supplementary Information (ESI) available: [details of any supplementary information available should be included here]. See DOI: 10.1039/x0xx00000x

systematic differences in alkyl side chain branching. It is well known that changes in branching in uncharged organic molecules yields different properties[36,37] and the effects on IL properties by altering side-chain branching have also been observed.[38] These changes in properties have been generally accounted for by the molecular architecture and its spatial arrangement. However, to our knowledge, no study has been performed to systematically isolate and evaluate how changes in the branching of otherwise isomeric side-chains influence the physical properties of ionic liquids. Certainly, a thorough knowledge of the effect of branched functional groups on the properties of ionic liquids will aid in their design.

To this end, we synthesized four structural isomers of ionic liquids with different isomeric propyl substituents on the 1,2,3-triazolium cation core as shown in Figure 1, all having the same bis(trifluoromethyl-sulfonyl)amide, Tf_2N^-, anion.

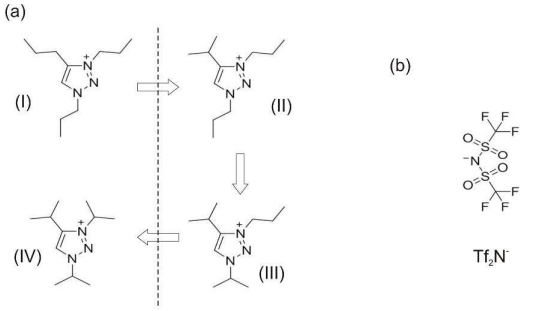

Figure 1. Ionic liquids (**I**) - (**IV**) studied here are comprised of 4 isomeric cations shown in (a) and common Tf_2N^- anion in (b). The isomeric cations each has 3 propyl side groups off of the 1,2,3-traizolium core; (**I**) has all linear *n*-propyl groups, and the clockwise progression to (**IV**) corresponds to the stepwise addition of branched isopropyl groups at the positions indicated. We study how various IL properties evolve with these rather subtle differences in cation structure as the number of branched side-chains changes. The dashed vertical line in (a) separates ILs (**I**) and (**IV**) having more symmetric cations with all *n*-propyl and all isopropyl side groups from (**II**) and (**III**) having less symmetric cations with mixed branched and linear side groups.

The number of branched side groups is systematically varied from 0 to 3 by replacing *n*-propyl with isopropyl groups yielding ILs (**I**) - (**IV**) as shown. Considering the similarity of the *n*-propyl and isopropyl groups, rather subtle structural differences exist between these samples. Indeed it might be expected that the interactions and resultant properties would be quite similar for these isomeric ILs, or possibly to vary linearly and systematically from IL(**I**) to IL(**IV**) with the number of branched alkyl side groups. We found a more complex variation in properties as the number of branched alkyl groups changes, with some scaling strongly with the number of branched side-chains, some scaling with the symmetry of the distribution of the side-chains, and others not strongly correlated with the differences in side chain isomerism. Below we present the results of various physical property measurements, and then a framework with which we reconcile their disparate trends with branching.

Results of property measurements

A range of properties were measured from this set of four ionic liquids. Phase transitions were characterized via modulated differential scanning calorimetry (MDSC)[39] and thermal stability was characterized by thermogravimetric analysis (TGA). Room temperature physical properties measured include density, viscosity, CO_2 uptake, diffusion, and ionic properties. Ionic property measurements include pulsed gradient spin echo nuclear magnetic resonance spectroscopy (PGSE-NMR) to determine ion self-diffusion and electrochemical impedance spectroscopy (EIS) to determine ionic conductivity in an electric field. Together these values determine the contribution of the diffusing species to the ion conductivity, with the ionicity giving the effective fraction of ion pairs that are dissociated.[40] Local molecular-orbital structure within the anion and cations was measured with Near Edge X-ray Absorption Fine Structure (NEXAFS) Spectroscopy. NEXAFS is less commonly applied to study ionic liquids, although it has been used to investigate local structural arrangements[41], interionic interactions[42], solvent-solute interactions[43], and electronic structure[44] of imidazolium-based ILs.

A description of the IL synthesis and the experimental procedures for each of these techniques is included in the Supporting Information (SI).

Phase transition temperatures - modulated DSC and TGA

MDSC results for these samples are dependent on scan rate and cycle number as shown in the SI. Figure 2 shows the second MDSC heating curves for these samples measured with scan rate of 1 °C/min.

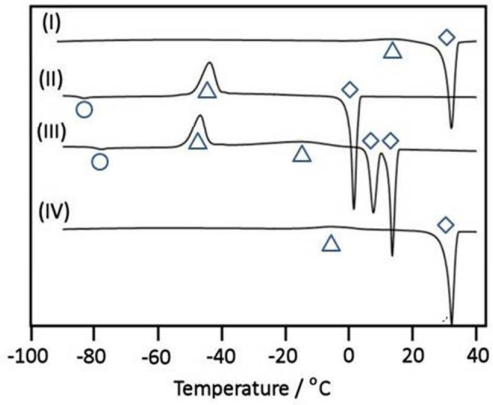

Figure 2. The second modulated DSC heating curves for the 4 ILs are vertically offset as noted, with exothermic events going upward. Labelled features include glass transitions (circles), exothermic events thought to be cold-crystallization (triangles), and melting transitions (diamonds). Other physical property measurements were made between 25-30 °C with all samples in a liquid state due to undercooling for (**I**) and (**IV**).

Scans are vertically offset for clarity and otherwise have the same vertical scale. Phase transitions observed include weak glass transitions (circles) for (**II**) and (**III**). Exothermic transitions thought to be cold-crystallization (triangles) are present for all samples, as are pronounced melting transitions (diamonds). The DSC trends for the ILs clearly do not scale with the number of branched side-chains. ILs (**I**) and (**IV**), with more symmetric cations, show very similar behaviour, with very weak cold crystallization peaks followed closely by comparable melting temperatures. Likewise, ILs (**II**) and (**III**), whose cations have mixed linear and branched side-chains, exhibit comparable thermal trends. Only ILs (**II**) and (**III**) exhibit weak glass transitions at ~ -80° C, followed by strong cold-crystallization peaks at ~ -50° C. IL (**III**) exhibits two cold crystallization and melting events, signalling that two distinct phases coexist in this sample during this measurement. From these data it is evident that ILs (**I**) and (**IV**) have a more stable phase below their melting temperatures than ILs (**II**) and (**III**). Furthermore, the phase stability of (**I**) and (**IV**) is quite comparable, indicating that the symmetry of the alkyl side-chains is more important than whether they are branched or not, at least for the interactions that determine these properties (Figure 2).

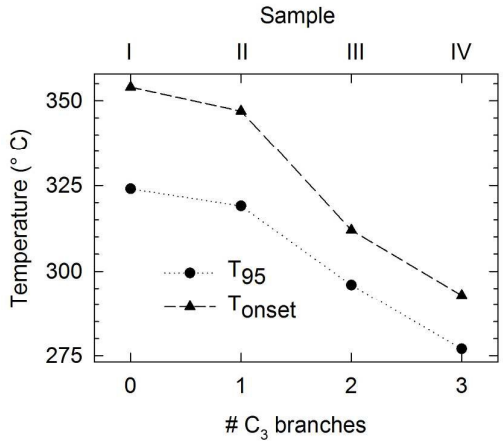

Figure 3. The results of thermogravimetric analysis for all samples as noted. T_{95} is the temperature where mass is reduced by 5% of initial mass at room T. T_{onset} is the temperature at onset of thermal decomposition. Both quantities decrease monotonically with the number of branched C_3 side-chains.

The TGA results in Figure 3 include the temperature at which the sample mass has decreased by 5% (T_{95}), and the temperature for the onset of rapid thermal decomposition (T_{onset}). These temperatures show a strong, linear dependence on the number of branched side-chains. Thus, the strongly thermally activated mechanisms promoting decomposition are apparently very different from those involved with the phase changes measured by DSC. We expect that these TGA trends are determined by thermal decomposition by the reverse Menshutkin reaction (dealkylation) possibly via both substitution and elimination reactions akin to the reported mechanism for imidazolium ILs with Tf_2N^- anion.[45] Depending upon the anion, imidazolium-based ILs are also observed to lose thermal stability with increased branching. [38,45–47]

Room temperature physical properties (density, viscosity, CO_2 uptake)

All property results presented below were made with the samples at 25 - 30° C in a viscous liquid state. While the MDSC results indicate that samples (**I**) and (**IV**) melt above 30° C, their thermal history prior to other property measurements rendered them liquid for these measurements.

The measured densities for the four ILs are shown in Figure 4a. IL **(I)** has the highest density in this series whereas (**II**), (**III**), and (**IV**) all have comparable densities. In analogy with polymers composed of linear and branched alkyl chains,[48] the higher density of (**I**) may result from more efficient ion packing, possibly including a more planar cation, on average, compared to ILs (**II**) - (**IV**). Evidently, a single branched side group is sufficient to disrupt this efficient packing. However, the density differences are slight.

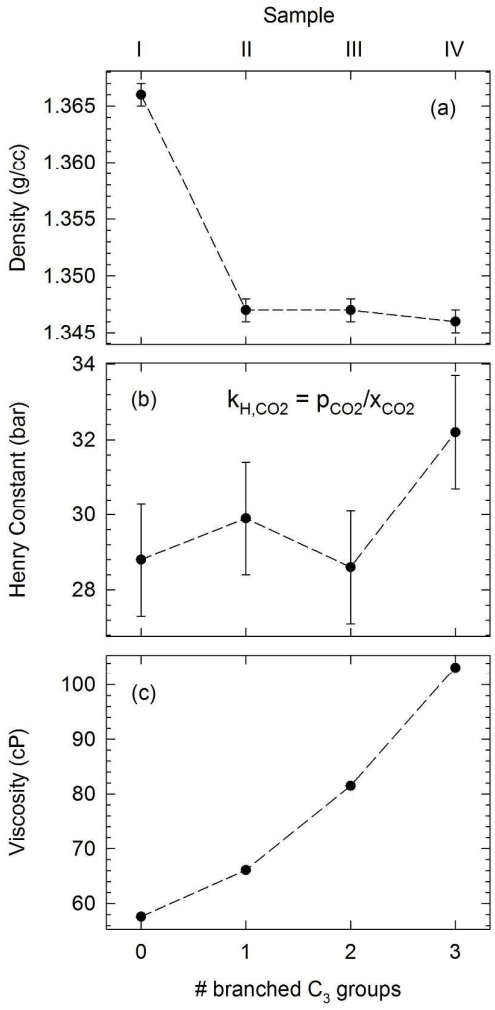

Figure 4. Room temperature properties for ILs (**I**) - (**IV**) include density (a), CO_2 uptake given by the inverse of the Henry's law constant (b), and viscosity (c). Only the viscosity shows a significant variation with the number of branched C_3 cation side-chains.

We note that *ab initio* calculations of densities as described in our earlier work[24] did not capture the measured density trends in ILs (**I**) - (**IV**). For side-groups with no branching such as ether, phenyl, and mixed groups, *ab initio* calculated densities reflected the same trend captured in the experiments.[24,32] This was not the case for the ILs studied here; evidently the short C_3 side groups yielding very small density differences, as opposed to larger groups yielding larger measured variation, render the same *ab initio* calculations less reliable to capture relative density trends.

The Henry's law constant for CO_2 uptake in Figure 4b exhibits weak, if any, variation across ILs (**I**) - (**IV**). The uptake may be somewhat smaller for IL (**IV**) than that of the others. It seems that, CO_2 uptake is determined by effective free volume but not free volume of the ionic liquid. Then it can be said that IL (**IV**) has lowest effective free volume available for CO_2 solvation. However, considering the large Henry's law constant error bars and weak variation in density this conclusion cannot be definitively confirmed. The only statistically significant difference is between in Henry constant is between IL (**I**) and (**IV**).

Distinctly different from the weak or absent variation in density and CO_2 uptake with the number of branched side groups in ILs (**I**) - (**IV**), the measured viscosity shows a very strong monotonic increase with the number of branched side-chains as seen in Figure 4c. The increase in viscosity with the number of branched isopropyl groups is similar to an increase with branching observed in imidazolium-based ILs,[49] and is easily explained mechanistically as an increase in the shear resistance to intermolecular motion as the number of more rigid and branched isopropyl cation groups increases. This type of increase in viscosity has also been observed in polymers and polymer melts,[50–52] as well as uncharged small molecules[53] with the introduction of similar steric effects reducing motion. In these triazolium-based cations, the results of steric and possibly other short-range interactions involving the C_3 groups need not be the same when they are operating between relatively stationary ions near potential energy minima versus interactions between ions in relative motion with respect to each other.

Ionic properties

Measurements of ionic properties were obtained from EIS and PFSE-NMR techniques described in the SI, and the results are displayed in Figure 5 where they are plotted vs. the number of branched side-chains.

Ionic conductivity measuring the net transport of (unpaired) ions in Figure 5a displays a pronounced decrease as the number of branched side-chain increases. This decrease is uniform and weak (~ 3%) across ILs (**I**) - (**III**), and much larger (~20%) from IL (**III**) to IL (**IV**). Cation and anion diffusion coefficients in Figure 5b obtained by NMR cannot distinguish between motion of paired and unpaired ions. The values obtained show a strong (~35 %), almost linear decrease with the increasing number of branched side-chains.

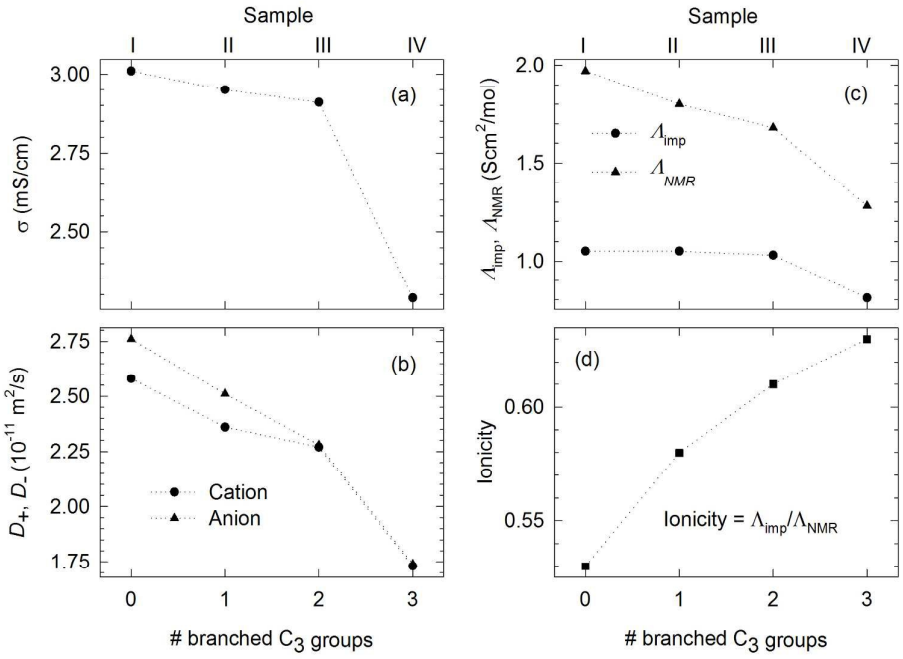

Figure 5. Measured ionic properties of ILs (I) - (IV) plotted vs the number of branched cation C_3 side-chains. (a) shows ionic conductivity, σ, measured via impedance spectroscopy. (b) shows cation (D_+) and anion (D_-) diffusion coefficients determined by fitting pulsed field NMR measurements. (c) shows molar conductivities determined from impedance measurements, Λ_{imp}, and from NMR, Λ_{NMR}. (d) shows the dimensionless ionicity given by $\Lambda_{imp}/\Lambda_{NMR}$. All measurements were made at 30° C. Dotted lines connect data points as guides to the eye.

Journal Name

ARTICLE

This is comparable in size to viscosity changes across ILs (**I**) to (**IV**), suggesting that similar mechanisms resulting from side chain branching limit the motion of ions in each case. As Λ_{imp} senses only the motion of unpaired ions, the ratio $\Lambda_{imp}/\Lambda_{NMR}$ gives the fraction of unpaired ions or the ionicity in Figure 5d. Ionicity increases systematically by roughly 20% with the number of branched side-chains. The values of ionicity indicate that somewhat more than half of the ion pairs are dissociated at any instant in time and fall within the range of values reported for other ILs.[29,40]

The meaning and mechanisms behind the ionicity concept remain an active topic of discussion. The ionicity results from the net balance of these effects. The 20% increase in ionicity across ILs (**I**) – (**IV**) show that the branched isopropyl groups have a systematic and mildly destabilizing effect in the cation-anion pairing interactions. Evidently, the same mechanisms that increase viscosity with branching do not solely determine ionicity trends, since they would promote reduced ionicity with branching. Of course the notion of two-body ion pairing and unpairing between cations and anions is oversimplified since it ignores the contribution of the long range coulombic interactions that promote structural correlation at all length scales.

Local molecular orbital structure from NEXAFS

Each of the properties discussed above senses a macroscopic average response, and while they may be interpreted in terms of microscopic intra- and intermolecular interactions between the cations and anions, they are not directly sensitive to the ionic structures and their interactions. Intraionic information from the ILs can be obtained with NEXAFS, which measures the strength of dipole transitions from core 1*s* states into 2*p* states that are hybridized into the local antibonding molecular orbital structure. By measuring the NEXAFS at the carbon, nitrogen, oxygen, and fluorine K edges, we obtain insight into the separate response of both ions to changes in cation side-chain branching.

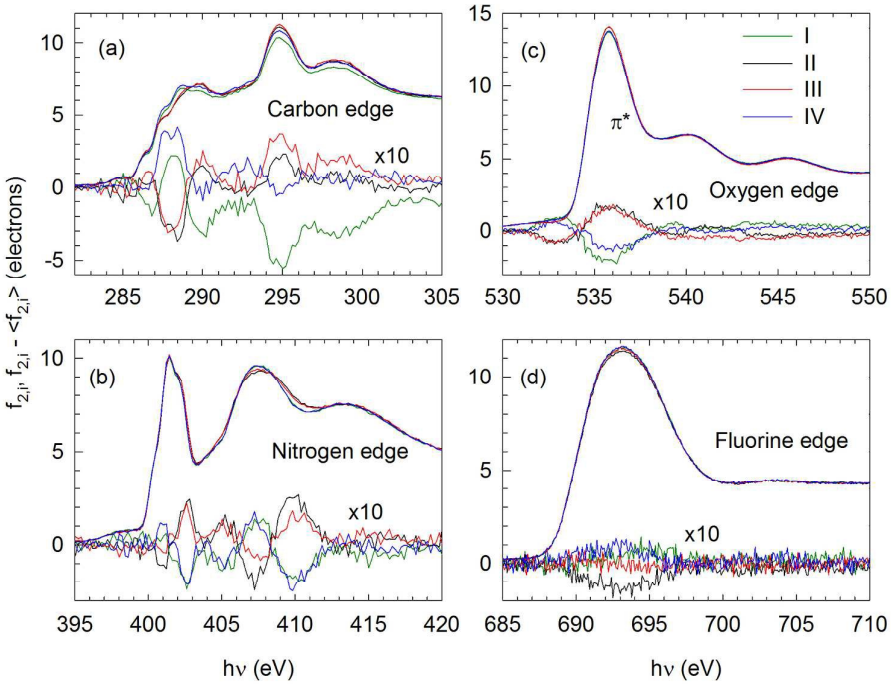

Figure 6. X-ray absorption spectra measured via total electron yield from ILs (**I**) - (**IV**) at the carbon (a), nitrogen (b), oxygen (c) and fluorine (d) K edges provide localized views of the antibonding molecular orbital structure around these species. Absorption spectra are normalized to the absolute scales of the atomic scattering factors (f_2) for intensity comparison. To highlight the subtle differences between spectra with changes in cation side-chains, each the average of all spectra is subtracted from each one and scaled by 10 in each panel.

The measured spectra, normalized to the imaginary part of the atomic scattering factor, f_2, from each edge are shown in Figure 6. Spectral differences between samples, though quite small, are robust. To magnify these differences, we also plot the difference between individual spectra and their averages scaled by 10 in the same panels. We note that considering the subtle propyl group changes between the four cation isomers, it is remarkable that systematic spectral differences are apparent. Since O and F are unique to the Tf_2N^- anion, which is common between all samples, any spectral changes between samples at these edges must be induced by changing interionic interactions due to the cation side chain branching. Clear evidence for NEXAFS sensitivity to changing cation-anion interactions with differing C_3 branching is apparent in the oxygen spectra (Figure 6c). The dominant features in the normalized f_2 spectra are the strong π* transitions at 535.6 eV and the weaker σ* transitions at higher energies. A weak pre-peak near 533 eV is also observed, and is more easily seen in the difference spectra than the normalized spectra themselves. A pairing of spectral features between samples in the difference spectra is obvious; the weak pre-peak is stronger for ILs (**I**) and (**IV**) than for ILs (**II**) and (**III**), while the strong π* peak is stronger for (**II**) and (**III**) than for (**I**) and (**IV**). This pairing suggests that cation symmetry is the main contributor to the spectral changes. The relative size of spectral changes with cation between ILs is better observed by plotting the difference spectra over the average, $(f_{2,i} - \langle f_{2,i}\rangle) / \langle f_{2,i}\rangle$ (see SI). The weak pre-peak intensity differs by over 20% between samples, while the strong π* peak difference is only 4%. This relative spectral difference between the ILs in the oxygen pre-peak between samples is the largest observed at all four absorption edges.

In contrast to the oxygen spectra, the fluorine spectra in Figure 6d exhibit insignificant spectral changes with changing cation side-chain branching. The fluorine spectra exhibit a broad σ* peak whose uniformity indicates that the chemical environment of the trifluoro groups is similar for all samples. These spectra correspond well with published fluorine NEXAFS of ILs pairing Li and imidazolium with Tf_2N^-.[42]

Considering the anion O and F spectra together, we understand the relatively strong O spectral changes to result because the oxygens are near the anion charge center and thus are expected to be strongly influenced by changing interactions with the cations. The triflouro groups are away from the charge center and, evidently, less actively involved in anion-cation interactions. Identifying specific cation-anion interactions that cause the O spectra to group according to cation symmetry is difficult from the spectral fingerprinting alone. Tf_2N^- is known to be highly flexible and take on both of its *cis* and *trans* conformations.[21,54–56] It is possible that a change in *cis*/*trans* ratio with cation symmetry explains trends in the O spectra. Alternatively, the stronger pre-peak could result from a change in H-bonding with the cation that is somehow promoted by cation symmetry. While other possible scenarios could account for the O spectral changes, it is certain that they result from cation-anion interactions that depend more on cation symmetry than on the number of its branched side groups.

C and N are present in both cations and anions; however, 85% and 75% of these atoms, respectively, are in the cations so that their spectral features are expected to be dominated by the cations. Since C and N spectra are dominated by species in the cations, it is reasonable to expect that their changes result from changes in the cation molecular orbital structure due to intramolecular side-chain differences. However, given the strong sensitivity of the O spectra to cation side chain branching through non-bonding interionic interactions, it is possible that such interactions also influence the C and N spectra.

The nitrogen spectra senses electronic structure around the three nitrogens in the triazolium rings and the lone apical nitrogen in the cation. The spectra exhibit a complex of several π* lines centered around 401.5 eV, a very weak pre-peak at 398 eV, and strong σ* peaks at 407.5 and 413 eV. The π* lines are expected to contain strong contributions from the three ring nitrogens, with each having a distinct line because of their different bonding and charge.[57] The anion N exhibits some π* character via the extended electronic structure in Tf_2N^-.[42] The asymmetry around this apical N may also account for the weak pre-peak due to *s-p* hybridization. All of the nitrogens are expected to have contributions in the regions of the 2 σ* peaks. The different spectra are dominated by the highest energy π* feature at 402.2 eV, which is stronger and possibly blue-shifted for ILs (**II**) and (**III**) having lower symmetry cations. The σ* peak at 407.5 eV decreases in intensity and broadens for these ILs, while the higher energy peak is nearly identical for all samples. It is impossible to attribute the spectral changes solely to the cation or changes in intermolecular interactions since the N atoms are located at the charge centers for both ions. On one hand, the spectral pairing between symmetric and asymmetric cations is similar to that at the O edge where it results from some form of anion distortion, and the triazolium ring is expected to be relatively stable, suggesting that anion interactions may be the source of differences at the N edge. However, two of the propyl groups where branching changes occur are bonded to ring N atoms, so that changes in branching can influence these directly. Additionally, the overall cation molecular orbital structure may change in response to the relative symmetry of its side groups.

Of the 11 carbons in the cations, 9 reside in the propyl side-chains so that C spectra should be especially sensitive to changing structure and interactions involving these groups. A complex of several poorly resolved lines is evident in the 287 - 290 eV region where C-H σ* lines exist.[58] All C-H bonds are in the cations and 90% in the alkyl groups. It is thus somewhat surprising that the pairing between symmetric/asymmetric cations persists in this region. As this symmetry pairing is shared by the anion O, it may be through specific hydrogen bonding interactions.[28,59] If hydrogen bonding between cation and anion is indicated by these spectra, they also indicate that such bonding may be influenced by the cation symmetry. In the C-C σ* peaks at 295 and 300 eV the trends between samples deviate more from the symmetric pairing, such that branched cations have systematically higher intensities than the non-branched cation (**I**). This trend is generally consistent with the previous observation that the 300 eV resonance increases in intensity for branched alkanes.[60]

Discussion of observed property trends with branching

To better understand the operative interactions leading to measured properties above, properties are categorized in Table 1 according to whether their dependence on the distribution of cation side-chains scales with the number of branched C_3 groups, the symmetry of the distribution of C_3 groups, or not clearly or strongly with either of these. The full variation of behaviours is observed. Viscosity, ionic properties, and high temperature TGA properties scale with branching. The DSC phase transition behaviour and the element-specific NEXAFS results clearly group according to the cation symmetry. Density and CO_2 uptake do not show strong trends with cation side chain branching.

The NEXAFS trends show that the anion molecular orbital structure responds to the symmetry of the cation. This indicates that intermolecular interactions are pronounced in the NEXAFS, and since the DSC also scales with the cation symmetry, we infer that intermolecular interactions are primarily responsible for the DSC trends as well. Arguments from this insight and assuming that the ions, interactions, and properties can be described by a complex, multidimensional, temperature-dependent potential surface allow us to reconcile much of the initially puzzling set of scaling behaviours in Table. 1.

Properties that scale with cation symmetry are understood to be dominated by the nature of the potential energy minima describing the relative positions and orientations of neighbouring cations and anions. In the solid phases the cations and anions are predominantly localized within relatively well-defined minima that describe the short and intermediate range order. DSC phase transition temperatures (Figure 2) essentially measure the onset of inter- and possibly intramolecular motions relative to potential energy surfaces describing these solid phases.

The heating curves show that ILs (**I**) and (**IV**) evolve similarly and with enhanced structural stability as temperature is increased compared to ILs (**II**) and (**III**). We hypothesize that the potential energy surfaces of ILs (**I**) and (**IV**) exhibit more symmetry with respect to azimuthal rotation about the triazolium ring axis and that this promotes larger degeneracy with respect to attractive nearest neighbour interactions and hence more structural stability in these systems compared to ILs (**II**) and (**III**).

The NEXAFS results reveal that the mechanisms by which more symmetric potential energy surfaces relative to cation axial rotation promote interionic structural stability extend into the liquid phase where a sizable fraction of ions are evidently unpaired, as seen from the ionicity data. However, even paired ions in the liquid regime are expected to be in dynamic equilibrium. The effects of thermal excitation in the liquid state presumably explain the small size of spectral differences in NEXAFS signals that average over all instantaneous configurations present. Evidently the scaling of liquid phase NEXAFS spectra according to cation symmetry results from the most tightly bound, solid-like, interionic configurations that are similar to those below the melting temperature that account for the DSC trends.

Table 1. Measured physical, thermal, and local electronic properties of the four ionic liquids having common Tf_2N^- anion and isomeric $TzC_3C_3C_3$ cations are categorized according to whether they scale with the number of branched C_3 side groups, the symmetry of the distribution of C_3 side groups, or neither.

Property	Scales with number of branched cation C_3 groups	Scales with symmetry of cation C_3 groups	Scales with neither (or mixed)
Density			X
Viscosity	X		
TGA temperatures	X		
Henry's constant (CO_2 uptake)			X
DSC phase behaviour		X	
Ion diffusivity	X		
Ionic conductivity	X		
Ionicity	X		
Local electronic structure (from NEXAFS)*		X	

Several properties exhibit pronounced scaling with the number of branched propyl side groups. These include viscosity, decomposition temperatures, and ionic properties including ion diffusivity, ionic conductivity, and ionicity. Within this set properties we can distinguish two subgroups. The first subgroup includes viscosity, ion diffusivity, and ionic conductivity that involve thermally excited molecular displacements of paired or unpaired ions over spatial extents comparable to ionic dimensions and separations, i.e., motions between potential energy minima. In this regime we would expect the more rigid, branched isopropyl groups to limit such motion through short-range entanglements or internal friction. The viscosity (Figure 4c) and ion diffusion coefficients (Figure 5b) increase and decrease respectively, with more branched cation side-chains as we would expect if branching hinders motion, and the amount of variation of these properties across ILs (**I**) to (**IV**) is comparable. The decrease in ionic conductivity with branching is also consistent with hindered interionic motion due to branching-induced friction even though its trend with branching is somewhat different than those of viscosity and ion diffusivity.

Ionicity itself constitutes the second subgroup. If ionicity were limited by the same branching effects as viscosity and diffusivity, we would expect increased branching to cause ionicity to decrease, opposite to what is observed. One possibility for the ionicity scaling is that, for the fraction of ions counted as unpaired, the branched isopropyl groups tend to limit the repairing into the most stable short-range configurations that underlie the symmetry scaling of DSC and NEXAFS results.

Density and CO_2 uptake listed in Table 1 are showing no clear or strong scaling trends with either the number of branched side groups or cation symmetry. While the density shows a measurable change from (**I**) to (**II**), the size of this change is very small compared to the systematic changes we've categorized in the other columns of Table 1. As discussed above, if density and CO_2 uptake depend primarily on the total free volume in the four ILs, they should scale together. The very subtle isomeric changes between n-propyl and isopropyl side groups is not expected to introduce significant changes in density or free volume, consistent with observations.

Conclusion

By preparing a set of four isomeric 1,2,3-traizolium based cations differing only by subtle variations in short propyl side-chains and measuring numerous physical properties of the resulting ionic liquids with a common Tf_2N^- anion, we are able to observe and correlate how different properties scale with systematic cation side chain branching. A full range of trends is observed, with some properties scaling with the number of branched alkyl side-groups, others with the symmetry of the distribution of the side-groups independent of whether they are branched or not, and still others largely uncorrelated with the cation side-groups changes. In essence we conclude that properties scaling with the symmetry of the distribution of cation side-chains are largely determined by short-range interionic interactions prevalent near the minima of complex, multidimensional potential energy surfaces. Furthermore, properties scaling with the number of branched isopropyl side chains are dominated by the large fraction of ions thermally excited out of these physical education minima and possibly transition from one minima to another.

It is clear that the property trends we observe here derive from the specific cations and anion constituting the ILs studied. The NEXAFS trends observed present a stringent test for efforts to model these ILs via *ab initio* methods, as the observed spectral differences are smaller than typical agreement between calculated and measured spectra even for model systems.

Acknowledgements

This technical effort was also performed in support of the U.S. Department of Energy's National Energy Technology Laboratory's on-going research on CO_2 capture under the contract DE-FE0004000.

References

1 Hallett, J. P.; Welton, T. Room-Temperature Ionic Liquids: Solvents for Synthesis and Catalysis. 2. *Chem. Rev.* **2011**, *111* (5), 3508–3576.
2 Welton, T. Room-Temperature Ionic Liquids. Solvents for Synthesis and Catalysis. *Chem. Rev.* **1999**, *99* (8), 2071–2084.
3 Smiglak, M.; Metlen, A.; Rogers, R. D. The Second Evolution of Ionic Liquids: From Solvents and Separations to Advanced Materials-Energetic Examples from the Ionic Liquid Cookbook. *Acc. Chem. Res.* **2007**, *40* (11), 1182–1192.
4 Rogers, R. D.; Seddon, K. R. Ionic Liquids - Solvents of the Future? *Science (80-.).* **2003**, *302* (5646), 792–793.
5 Plechkova, N. V; Seddon, K. R. Applications of Ionic Liquids in the Chemical Industry. *Chem. Soc. Rev.* **2008**, *37* (1), 123–150.
6 Shi, W.; Myers, C. R.; Luebke, D. R.; Steckel, J. A.; Sorescu, D. C. Theoretical and Experimental Studies of CO2 and H2 Separation Using the 1-Ethyl-3-Methylimidazolium Acetate ([emim][CH3COO]) Ionic Liquid. *J. Phys. Chem. B* **2012**, *116* (1), 283–295.
7 Wang, H.; Gurau, G.; Rogers, R. D. Ionic Liquid Processing of Cellulose. *Chem. Soc. Rev.* **2012**, *41* (4), 1519–1537.
8 Noda, A.; Susan, A. B.; Kudo, K.; Mitsushima, S.; Hayamizu, K.; Watanabe, M. Bronsted Acid-Base Ionic Liquids as Proton-Conducting Nonaqueous Electrolytes. *J. Phys. Chem. B* **2003**, *107* (17), 4024–4033.
9 Xiang, H. F.; Yin, B.; Wang, H.; Lin, H. W.; Ge, X. W.; Xie, S.; Chen, C. H. Improving Electrochemical Properties of Room Temperature Ionic Liquid (RTIL) Based Electrolyte for Li-Ion Batteries. *Electrochim. Acta* **2010**, *55* (18), 5204–5209.
10 Shi, W.; Sorescu, D. C.; Luebke, D. R.; Keller, M. J.; Wickramanayake, S. Molecular Simulations and Experimental Studies of Solubility and Diffusivity for Pure and Mixed Gases of H-2, CO2, and Ar Absorbed in the Ionic Liquid 1-N-Hexyl-3-Methylimidazolium Bis(Trifluoromethylsulfonyl)amide (Hmim Tf2N). *J. Phys. Chem. B* **2010**, *114* (19), 6531–6541.
11 Mikkelsen, M.; Jorgensen, M.; Krebs, F. C. The Teraton Challenge. A Review of Fixation and Transformation of Carbon Dioxide. *Energy Environ. Sci.* **2010**, *3* (1), 43–81.
12 Wang, C. M.; Luo, X. Y.; Luo, H. M.; Jiang, D. E.; Li, H. R.; Dai, S. Tuning the Basicity of Ionic Liquids for Equimolar CO2 Capture. *Angew. Chemie-International Ed.* **2011**, *50* (21), 4918–4922.
13 Tokuda, H.; Ishii, K.; Susan, M. A. B. H.; Tsuzuki, S.; Hayamizu, K.; Watanabe, M. Physicochemical Properties and Structures of Room-Temperature Ionic Liquids. 3. Variation of Cationic Structures. *J. Phys. Chem. B* **2006**, *110* (6), 2833–2839.
14 Tokuda, H.; Hayamizu, K.; Ishii, K.; Susan, M. A. B. H.; Watanabe, M. Physicochemical Properties and Structures of Room Temperature Ionic Liquids. 1. Variation of Anionic Species. *J. Phys. Chem. B* **2004**, *108* (42), 16593–16600.
15 Tokuda, H.; Hayamizu, K.; Ishii, K.; Susan, M. A. B. H.; Watanabe, M. Physicochemical Properties and Structures of Room Temperature Ionic Liquids. 2. Variation of Alkyl Chain Length in Imidazolium Cation. *J. Phys. Chem. B* **2005**, *109* (13), 6103–6110.
16 Stoppa, A.; Zech, O.; Kunz, W.; Buchner, R. The Conductivity of Imidazolium-Based Ionic Liquids from (−35 to 195) °C. A. Variation of Cation's Alkyl Chain †. *J. Chem. Eng. Data* **2010**, *55* (5), 1768–1773.
17 Fletcher, K. A.; Baker, S. N.; Baker, G. A.; Pandey, S. Probing Solute and Solvent Interactions within Binary Ionic Liquid mixturesThis Paper Is Dedicated with Congratulations to Professor Frank V. Bright, Recipient of the 2003 New York SAS Gold Medal Award. *New J. Chem.* **2003**, *27* (12), 1706.
18 Umebayashi, Y.; Fujimori, T.; Sukizaki, T.; Asada, M.; Fujii, K.; Kanzaki, R.; Ishiguro, S.-I. Evidence of Conformational Equilibrium of 1-Ethyl-3-Methylimidazolium in Its Ionic Liquid Salts: Raman Spectroscopic Study and Quantum Chemical Calculations. *J. Phys. Chem. A* **2005**, *109* (40), 8976–8982.
19 Xue, L.; Padgett, C. W.; DesMarteau, D. D.; Pennington, W. T. Synthesis and Structures of Alkali Metal Salts of Bis[(trifluoromethyl)sulfonyl]imide. *Solid State Sci.* **2002**, *4* (11-12), 1535–1545.
20 Martinelli, A.; Matic, A.; Johansson, P.; Jacobsson, P.; Börjesson, L.; Fernicola, A.; Panero, S.; Scrosati, B.; Ohno, H. Conformational Evolution of TFSI− in Protic and Aprotic Ionic Liquids. *J. Raman Spectrosc.* **2011**, *42* (3), 522–528.
21 Lassègues, J. C.; Grondin, J.; Holomb, R.; Johansson, P. Raman Andab Initio Study of the Conformational Isomerism

in the 1-Ethyl-3-Methyl-Imidazolium Bis(trifluoromethanesulfonyl)imide Ionic Liquid. *J. Raman Spectrosc.* **2007**, *38* (5), 551–558.

22 Watkins, J. D.; Roth, E. A.; Lartey, M.; Albenze, E.; Zhong, M.; Luebke, D. R.; Nulwala, H. B. Ionic Liquid Regioisomers: Structure Effect on the Thermal and Physical Properties. *New J. Chem.* **2015**, *39* (3), 1563–1566.

23 Nulwala, H. B.; Tang, C. N.; Kail, B. W.; Damodaran, K.; Kaur, P.; Wickramanayake, S.; Shi, W.; Luebke, D. R. Probing the Structure-Property Relationship of Regioisomeric Ionic Liquids with Click Chemistry. *Green Chem.* **2011**, *13* (12), 3345.

24 Yan, F.; Lartey, M.; Damodaran, K.; Albenze, E.; Thompson, R. L.; Kim, J.; Haranczyk, M.; Nulwala, H. B.; Luebke, D. R.; Smit, B. Understanding the Effect of Side Groups in Ionic Liquids on Carbon-Capture Properties: A Combined Experimental and Theoretical Effort. *Phys. Chem. Chem. Phys.* **2013**, *15* (9), 3264–3272.

25 Obadia, M. M.; Mudraboyina, B. P.; Allaoua, I.; Haddane, A.; Montarnal, D.; Serghei, A.; Drockenmuller, E. Accelerated Solvent- and Catalyst-Free Synthesis of 1,2,3-Triazolium-Based Poly(Ionic Liquid)s. *Macromol. Rapid Commun.* **2014**, *35* (8), 794–800.

26 Mukai, T.; Nishikawa, K. 4,5-Dihaloimidazolium-Based Ionic Liquids: Effects of Halogen-Bonding on Crystal Structures and Ionic Conductivity. *RSC Adv.* **2013**, *3* (43), 19952.

27 Hunt, P. a. Why Does a Reduction in Hydrogen Bonding Lead to an Increase in Viscosity for the 1-Butyl-2,3-Dimethyl-Imidazolium-Based Ionic Liquids? *J. Phys. Chem. B* **2007**, *111* (18), 4844–4853.

28 Fumino, K.; Peppel, T.; Geppert-Rybczyńska, M.; Zaitsau, D. H.; Lehmann, J. K.; Verevkin, S. P.; Köckerling, M.; Ludwig, R. The Influence of Hydrogen Bonding on the Physical Properties of Ionic Liquids. *Phys. Chem. Chem. Phys.* **2011**, *13* (31), 14064–14075.

29 Ueno, K.; Tokuda, H.; Watanabe, M. Ionicity in Ionic Liquids: Correlation with Ionic Structure and Physicochemical Properties. *Phys. Chem. Chem. Phys.* **2010**, *12* (8), 1649–1658.

30 Mao, J. X.; Nulwala, H. B.; Luebke, D. R.; Damodaran, K. Spectroscopic and Computational Analysis of the Molecular Interactions in the Ionic Liquid Ion Pair [BMP]+[TFSI]−. *J. Mol. Liq.* **2012**, *175*, 141–147.

31 Mao, J. X.; Lee, A. S.; Kitchin, J. R.; Nulwala, H. B.; Luebke, D. R.; Damodaran, K. Interactions in 1-Ethyl-3-Methyl Imidazolium Tetracyanoborate Ion Pair: Spectroscopic and Density Functional Study. *J. Mol. Struct.* **2013**, *1038*, 12–18.

32 Yan, F.; Lartey, M.; Jariwala, K.; Bowser, S.; Damodaran, K.; Albenze, E.; Luebke, D. R.; Nulwala, H. B.; Smit, B.; Haranczyk, M. Toward a Materials Genome Approach for Ionic Liquids: Synthesis Guided by Ab Initio Property Maps. *J. Phys. Chem. B* **2014**, *118* (47), 13609–13620.

33 Hanelt, S.; Liebscher, J. A Novel and Versatile Access to Task-Specific Ionic Liquids Based on 1,2,3-Triazolium Salts. *Synlett* **2008**, *2008* (7), 1058–1060.

34 Kolb, H. C.; Finn, M. G.; Sharpless, K. B. Click Chemistry: Diverse Chemical Function from a Few Good Reactions. *Angew. Chem. Int. Ed. Engl.* **2001**, *40* (11), 2004–2021.

35 Sanghi, S.; Willett, E.; Versek, C.; Tuominen, M.; Coughlin, E. B. Physicochemical Properties of 1,2,3-Triazolium Ionic Liquids. *RSC Adv.* **2012**, *2* (3), 848.

36 Cohen, J. B. *Organic Chemistry for Advanced Students, Volume 1*; Edward Arnold, 1907.

37 *Ullmann's Fine Chemicals, 3 Volume Set*; Wiley, 2013.

38 Erdmenger, T.; Vitz, J.; Wiesbrock, F.; Schubert, U. S. Influence of Different Branched Alkyl Side Chains on the Properties of Imidazolium-Based Ionic Liquids. *J. Mater. Chem.* **2008**, *18* (43), 5267.

39 Jin, L.; Nairn, K. M.; Forsyth, C. M.; Seeber, A. J.; MacFarlane, D. R.; Howlett, P. C.; Forsyth, M.; Pringle, J. M. Structure and Transport Properties of a Plastic Crystal Ion Conductor: Diethyl(methyl)(isobutyl)phosphonium Hexafluorophosphate. *J. Am. Chem. Soc.* **2012**, *134* (23), 9688–9697.

40 MacFarlane, D. R.; Forsyth, M.; Izgorodina, E. I.; Abbott, A. P.; Annat, G.; Fraser, K. On the Concept of Ionicity in Ionic Liquids. *Phys. Chem. Chem. Phys.* **2009**, *11* (25), 4962–4967.

41 Zitolo, A.; Migliorati, V.; Aquilanti, G.; D'Angelo, P. On the Possibility of Using XANES to Investigate Bromide-Based Ionic Liquids. *Chem. Phys. Lett.* **2014**, *591*, 32–36.

42 Rodrigues, F.; Galante, D.; do Nascimento, G. M.; Santos, P. S. Interionic Interactions in Imidazolic Ionic Liquids Probed by Soft X-Ray Absorption Spectroscopy. *J. Phys. Chem. B* **2012**, *116* (5), 1491–1498.

43 Rodrigues, F.; do Nascimento, G. M.; Santos, P. S. Studies of Ionic Liquid Solutions by Soft X-Ray Absorption Spectroscopy. *J. Electron Spectros. Relat. Phenomena* **2007**, *155* (1-3), 148–154.

44 Nishi, T.; Iwahashi, T.; Yamane, H.; Ouchi, Y.; Kanai, K.; Seki, K. Electronic Structures of Ionic Liquids and Studied by Ultraviolet Photoemission, Inverse Photoemission, and near-Edge X-Ray Absorption Fine Structure Spectroscopies. *Chem. Phys. Lett.* **2008**, *455* (4-6), 213–217.

45 Maton, C.; De Vos, N.; Stevens, C. V. Ionic Liquid Thermal Stabilities: Decomposition Mechanisms and Analysis Tools. *Chem. Soc. Rev.* **2013**, *42* (13), 5963–5977.

46 Fredlake, C. P.; Crosthwaite, J. M.; Hert, D. G.; Aki, S. N. V. K.; Brennecke, J. F. Thermophysical Properties of Imidazolium-Based Ionic Liquids. *J. Chem. Eng. Data* **2004**, *49* (4), 954–964.

47 Awad, W. H.; Gilman, J. W.; Nyden, M.; Harris, R. H.; Sutto, T. E.; Callahan, J.; Trulove, P. C.; DeLong, H. C.; Fox, D. M. Thermal Degradation Studies of Alkyl-Imidazolium Salts and Their Application in Nanocomposites. *Thermochim. Acta* **2004**, *409* (1), 3–11.

48 Odian, G. *Principles of Polymerization*, 4th Editio.; Wiley-interscience, 2004.

49 Swartling, D.; Ray, L.; Compton, S.; Ensor, D. Preliminary Investigation into Modification of Ionic Liquids to Improve Extraction Parameters. *SAAS Bull. Biochem. Biotech.* **2000**, *13*, 1–7.

50 Stadler, F. J.; Mahmoudi, T. Understanding the Effect of Short-Chain Branches by Analyzing Viscosity Functions of Linear and Short-Chain Branched Polyethylenes. *Korea-Australia Rheol. J.* **2012**, *23* (4), 185–193.

51 Moore, L. D. Relations among Melt Viscosity, Solution Viscosity, Molecular Weight, and Long-Chain Branching in Polyethylene. *J. Polym. Sci.* **1959**, *36* (130), 155–172.

52 Busse, W. F.; Longworth, R. Effect of Molecular Weight Distribution and Branching on the Viscosity of Polyethylene Melts. *J. Polym. Sci.* **1962**, *58* (166), 49–69.

53 Lide, D. R. *CRC Handbook of Chemistry and Physics*; CRC Press, 1998.

54 Hardacre, C.; Holbrey, J. D.; Nieuwenhuyzen, M.; Youngs, T. G. A. Structure and Solvation in Ionic Liquids. *Acc. Chem. Res.* **2007**, *40* (11), 1146–1155.

55 Nakajima, K.; Oshima, S.; Suzuki, M.; Kimura, K. Surface Structures of Equimolar Mixtures of Imidazolium-Based Ionic Liquids Using High-Resolution Rutherford Backscattering Spectroscopy. *Surf. Sci.* **2012**, *606* (21-22), 1693–1699.

56 Holbrey, J. D.; Reichert, W. M.; Rogers, R. D. Crystal Structures of Imidazolium Bis(trifluoromethanesulfonyl)imide "Ionic Liquid" Salts: The First Organic Salt with a Cis-TFSI Anion Conformation. *Dalton Trans.* **2004**, No. 15, 2267–2271.

57 Darlatt, E.; Nefedov, A.; Traulsen, C. H.-H.; Poppenberg, J.; Richter, S.; Dietrich, P. M.; Lippitz, A.; Illgen, R.; Kühn, J.; Schalley, C. a.; et al. Interpretation of Experimental N K NEXAFS of Azide, 1,2,3-Triazole and Terpyridyl Groups by DFT Spectrum Simulations. *J. Electron Spectros. Relat. Phenomena* **2012**, *185* (12), 621–624.
58 Schöll, A.; Fink, R.; Umbach, E.; Mitchell, G. E.; Urquhart, S. G.; Ade, H. Towards a Detailed Understanding of the NEXAFS Spectra of Bulk Polyethylene Copolymers and Related Alkanes. *Chem. Phys. Lett.* **2003**, *370* (5-6), 834–841.
59 Hitchcock, P. B.; Seddon, K. R.; Welton, T. Hydrogen-Bond Acceptor Abilities of tetrachlorometalate(II) Complexes in Ionic Liquids. *J. Chem. Soc. Dalt. Trans.* **1993**, No. 17, 2639.
60 Hitchcock, A. P.; Ishii, I. Carbon K-Shell Excitation Spectra of Linear and Branched Alkanes. *J. Electron Spectros. Relat. Phenomena* **1987**, *42* (1), 11–26.